Hindawi
Advances in Civil Engineering
Volume 2024, Article ID 8263261, 19 pages
https://doi.org/10.1155/2024/8263261

Research Article

Feasibility Study of Expanded Clay Aggregate Lightweight Concrete for Nonstructural Applications

Shayan Ali Khan,[1,2] **Fazal Hussain**,[3] **Rao Arsalan Khushnood**,[4,5] **Hassan Amjad**,[2] **and Farhan Ahmad**[6]

[1]*Newmark Civil Engineering Lab, University of Illinois at Urbana–Champaign, 205 North Matthews Avenue, Urbana 61801, IL, USA*
[2]*NUST Institute of Civil Engineering (NICE), School of Civil and Environmental Engineering (SCEE), National University of Sciences and Technology (NUST), Sector H−12, Islamabad 44000, Pakistan*
[3]*College of Engineering and Computer Science, Texas A&M University Corpus Christi, 6300 Ocean Dr, Corpus Christi 78412, TX, USA*
[4]*Tunneling Institute of Pakistan, Shakarparian 44000, Islamabad, Pakistan*
[5]*Department of Structural, Geotechnical and Building Engineering, Politecnico di Torino, Corso Duca degli Abruzzi 24, Turin 10129, Italy*
[6]*School of Engineering, Design and Built Environment, Western Sydney University, Penrith 2751, NSW, Australia*

Correspondence should be addressed to Farhan Ahmad; f.ahmad@westernsydney.edu.au

Received 13 November 2023; Revised 7 February 2024; Accepted 9 February 2024; Published 29 February 2024

Academic Editor: Adewumi Babafemi

In nonstructural infill panels, common materials like expanded polystyrene panels face fire susceptibility, autoclaved aerated concrete (AAC) incurs high production costs, and traditional bricks come with a significant carbon footprint and weight. So, there is a requirement for infill panels that are not just resilient and lightweight but sustainable as well. This study seeks to address these issues by introducing sustainable and lightweight expanded clay aggregate (ECA) in concrete. Firstly, eight ECA mix designs were prepared by integrating fly ash and kerosene with clay, and ECA with a bulk density of 0.59 g/cm³ and compressive strength of up to 1.73 MPa were prepared. The lightest ECA mix was then chosen to explore their use in lightweight aggregate concrete (LWAC) along with fly ash as a secondary cementitious material. The resulting LWAC had a minimum density of 1,050 kg/m³ and a compressive strength of 6.8 MPa, fulfilling the standard requirements of a minimum of 3.5 MPa for nonstructural concrete.

1. Introduction

Due to the outstanding performance and functional advantages of lightweight aggregates (LWAs), they are growing in demand. These aggregates, whether they occur naturally or are synthesized artificially, possess a density lower than 0.88 g/cm^3, as defined by ASTM C-330 [1]. Their distinct lightweight properties stem from a porous, spongy structure and nearly all natural LWAs are of extrusive origin [2]. Additionally, a diverse range of artificial aggregates i.e., fly ash, blast furnace slag, coal ash, and crushed bricks are also prevalent [3].

Expanded clay aggregate (ECA) is also an artificial aggregate made by bloating clay, shale, or slate at temperatures ranging from 900 to 1,250°C [4]. It was patented as Haydite in 1917 and used in the SS Selma construction in 1919. Since then, it has been used for manufacturing lightweight concrete throughout the world.

Considerable research has been conducted to determine the optimal bloating zones, mechanisms, and the feasibility of various clays to undergo bloating [4–10]. However, the mix design of LWAs with expanded clay is still to be explored. For the first time Sivakumar and Kameshwari [11] mixed bottom ash with clay to synthesize ECAs and observed the impact of it on the mechanical properties of concrete made with these aggregates. Bottom ash was combined with clay in different proportions, and an increase in fly ash content enhanced the compressive, tensile, and flexural strength of concrete made

with these aggregates. Burbano-Garcia et al. [12] investigated the impact of waste engine oil on the physical and mechanical properties of ECA. This was very detailed research where the response of aggregates was observed by varying the waste engine oil doses (0%–2%), thermal cycles, and pellet sizes. It was observed that the compressive strength of aggregate with 2% oil came out to be 2.87 MPa, which outclassed that of conventional ECA 1.5 MPa. The lightweight concrete made from aggregates with 2% waste engine oil showed an astounding 19 MPa strength and 1,980 kg/m^3 density.

One of the main concerns of ECA is its manufacturing cost. This may be addressed by including industrial wastes in the mix design, which will reduce manufacturing costs and improve the aggregates' sustainability and environmental footprint. Vilarinho et al. [13] incorporated different industrial wastes, i.e., steel shot blasting dust (SBD), green liquor dregs (DRG), slaker grits, biomass ashes, sludges from wastewater treatment resulting from aluminum anodizing processes, from steel pickling processes (SSP), from galvanic processes (SG), sludges from urban wastewater treatment, slags, refractories, greensand (GSD) and core sand (CSD). They intended to study these additives' impact on aggregates' mechanical properties [13]. They found out that the aggregate made by the replacement of clay with wastes of SSP showed the least density of 373 kg/m^3, and those made by replacing clay with DRG showed a crushing strength of 1.5 MPa. Lee [14] further opened a new domain by adding kerosene as a bloating agent in the mix design of aggregates. This study indicated that an increase in bloating agents such as kerosene results in aggregates of reduced density. With the rise in kerosene content, the difference in partial pressures of carbon dioxide (CO_2), carbon monoxide (CO), and oxygen (O_2) increased which enhanced gasification inside the aggregates, ultimately forming lightweight and cellular aggregates.

On the other hand, lightweight aggregate concrete (LWAC) has brought revolution due to its enhanced properties, and ECA is one of the most predominantly used LWAs in LWAC. ECA-based LWAC saves up to 20% in steel when used in structural elements [15, 16]. When used for insulation or nonstructural infill panels, they reduce energy requirements for insulation by up to 50% [17–20]. Bricks are responsible for a significant amount of carbon emissions globally and in Bangladesh over 17% of their total annual CO_2 emissions are from brick kilns [21]. Infill wall panels i.e., lightweight expanded polystyrene beads (EPS) panels have revolutionized the world but have very less compressive strength, even less than the minimum 3.45 MPa requirement of nonstructural concrete masonry by ASTM C-129 [22]. Autoclaved aerated concrete (AAC) on the other hands need cutting edge technology to be manufactured therefore have very high cost [23]. Therefore, there is a requirement of sustainable, cheap, and easy to manufacture infill panels especially for the markets of developing countries.

This research aims to investigate the merits of kerosene as a bloating agent and fly ash in ECA and study the feasibility of their use for LWAC for Infill panels. The kerosene component facilitates the bloating mechanism through gasification, whereas adding fly ash augments sustainability since fly ash disposal is a concern for many countries. Kerosene, as compared to other petroleum products, is the best option as a bloating agent because it has a higher combustion efficiency and results in fewer products of incomplete combustion [10, 24]. Also, kerosene is cheaper than other potential petroleum products that might be used as bloating agents [25]. On the other hand, the global fly ash market has surged from USD 12.25 billion in 2021 to USD 19.19 billion in June 2022, says the market research report by Fortune Business Insights. Research by SkyQuest even claims that global fly ash production will reach 1.04 billion tons by 2030 [26]. That's why the researchers found it pertinent to integrate fly ash and kerosene in ECA and see their impact on ECA's mechanical properties, particularly density and crushing strength. In addition to ECA, the authors replaced a portion of cement with fly ash to propose a lightweight and sustainable mix design for nonstructural applications. Fly ash, known for reducing density in LWAC, enhances early strength through a filler effect and long-term strength by providing external lime and inducing pozzolanic reactions [27]. Replacing up to 35% of cement with fly ash increases LWAC workability by 31% compared to control samples, although this may result in reduced segregation resistance [28].

Table 1: Elemental composition of cement (%, wt).

Cement type	Oxides							
	CaO	SiO_2	Al_2O_3	Fe_2O_3	MgO	SO_3	Na_2O	K_2O
OPC	63.2	22.2	5.19	3.1	0.98	2.5	0.25	0.2

In this study, clay samples from Nandipur, Pakistan, were collected, crushed, and mixed with fly ash, kerosene, and water to formulate a ECA mix. ECA with fly ash and kerosene exhibited significantly lower weight than pure clay and fly ash aggregates. Scanning electron microscopy (SEM) revealed a more vesicular interior structure in these ECA's, meeting minimal density and strength standards for concrete use. Energy dispersive X-ray analysis indicated changes in elemental composition, with additional peaks in aggregates containing fly ash. ECA applications were further assessed in nonstructural concrete, emphasizing carbon emission reduction through partial cement replacement with fly ash (30%, 50%, and 70%). Comprehensive tests for nonstructural masonry requirements were conducted.

2. Materials and Methodology

2.1. Raw Materials. Clay samples were meticulously collected from Nandipur, a city in the southern region of Punjab province, Pakistan, ensuring extraction from a depth of approximately 1 m to maintain purity [29]. Addressing the unique context of Pakistan's industrial landscape, where textile mills contribute significantly to fly ash production, Class C fly ash complying to the standards of ASTM C-618 [30] was procured from Gul Ahmed Textile Mills Limited, Rawat, Islamabad. Additionally, kerosene, a vital component in the study, was sourced from Shell Petroleum company. Kohat cement of Grade 1 was used in this study and the cement complied to all the specifications of ASTM C-93 [31]. The elemental composition of cement is shown in Table 1.

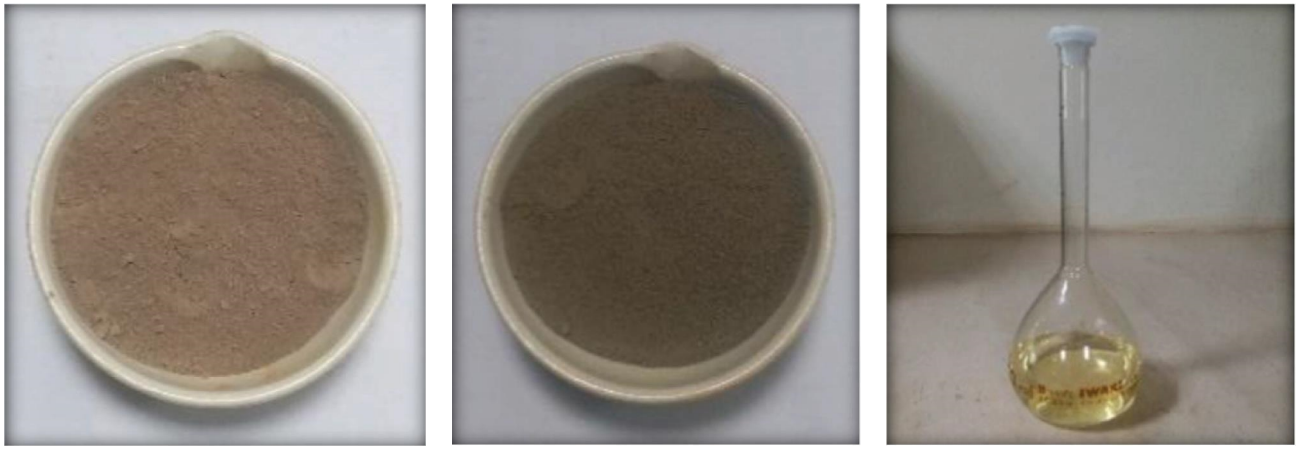

(a) (b) (c)

Figure 1: Raw material used for ECA synthesis: (a) Nandipur clay, (b) fly ash, and (c) kerosene oil.

Table 2: Mix designs of ECA.

Clay recipes	PS (mm)	Clay quantity (g)	FA (%)	K (%)
PC	15	150	0	0
CF1	15	146	5	0
CF2	15	142	10	0
CF3	15	138	15	0
CK1	15	150	0	3
CK2	15	150	0	6
CFK1	15	146	5	2
CFK2	15	142	10	4

K = kerosene oil (%), PS = pellet size (mm), and FA = fly ash (%wt. of clay).

Figure 1. shows the physical appearance of raw materials used for ECA.

2.2. Mix Design of ECA. As already noted, the rationale for blending kerosene and fly ash is the synthesis of environmental friendly and readily bloatable ECA. The experimental strategy was established in such a manner that the aggregates were classified into four major groups, namely pure clay (PC), clay with fly ash (CF), clay with kerosene (CK), and lastly, both kerosene and fly ash (CKF). This categorization aimed to effectively comprehend the results of combining kerosene and fly ash and determine the distinctions between their individual applications. The mix designs of ECA are summarized in Table 2.

After the acquisition of pure clay, the mineralogy of the clay was examined through an X-ray diffraction (XRD) test. It was also necessary to find the exact chemical composition of clay and fly ash. The chemical composition of clay and fly ash was determined using an X-ray fluorescence (XRF) test. The main goal of this test was to locate the clay on the Riley diagram [32] so that the potential of the clay for bloating could be determined. To determine the Atterberg limits and the optimal moisture content (W_{op}) of the clay essential geotechnical investigation has been conducted. This allowed the precise amount of water to be added for the best bloating of aggregate. Table 2 shows the fundamental geotechnical properties of the clay under study ASTM D-4318 was employed to find the plastic limit (PL), liquid limit (LL), and plasticity index (PI) of the clay [33]. While ASTM D-427 was used to find the shrinkage limit (SL) [34]. Equations (1) and (2) were taken into consideration to determine PI and SL. An equation has been formulated by Moreno-Maroto and Alonso-Azcárate [35] which has been depicted as Equation (3) below was used to determine the maximum toughness (T_{max}) in kilojoules per cubic meter (KJ/m³) based on clay's PI and LL. The trials were planned such that the difference between aggregates having no additives, solely fly ash as an additive, only kerosene as a bloating agent, and eventually both fly ash and kerosene could be effectively evaluated. The fly ash replacement of clay percentage was changed from 0% to 15% with a difference of 5% of the total clay weight while keeping the kerosene content at 0%. Then, kerosene oil was added in concentrations ranging from 0% to 6%, with 3% of the water weight. Finally, the fly ash concentration was modulated from 0% to 10% by changing the kerosene percentage from 0% to 4%.

$$\mathrm{PI} = \mathrm{LL} - \mathrm{PL}, \tag{1}$$

$$\mathrm{SL} = \left(\frac{m_1 - m_2}{m_2}\right)(100) - \left[\frac{(V_i - V_f)\rho_w}{m_2}\right](100), \tag{2}$$

$$T_{max} = \frac{\left[\frac{\mathrm{PI}}{\mathrm{LL}} - 0.3397\right]}{0.0077}, \tag{3}$$

$$W_{optimal} = PL \times 1.234. \tag{4}$$

2.3. LWA Manufacturing. Following this preliminary testing, ECA synthesis was undertaken. ECA synthesis comprises two steps majorly i.e., pelletization and bloating. In the pelletization stage, clay was first crushed into fine particles. For grinding, the Los Angeles apparatus was used with eight steel balls [36]. The optimal moisture content (W_{op}, %) required to achieve optimal workability for molding clay pellets was

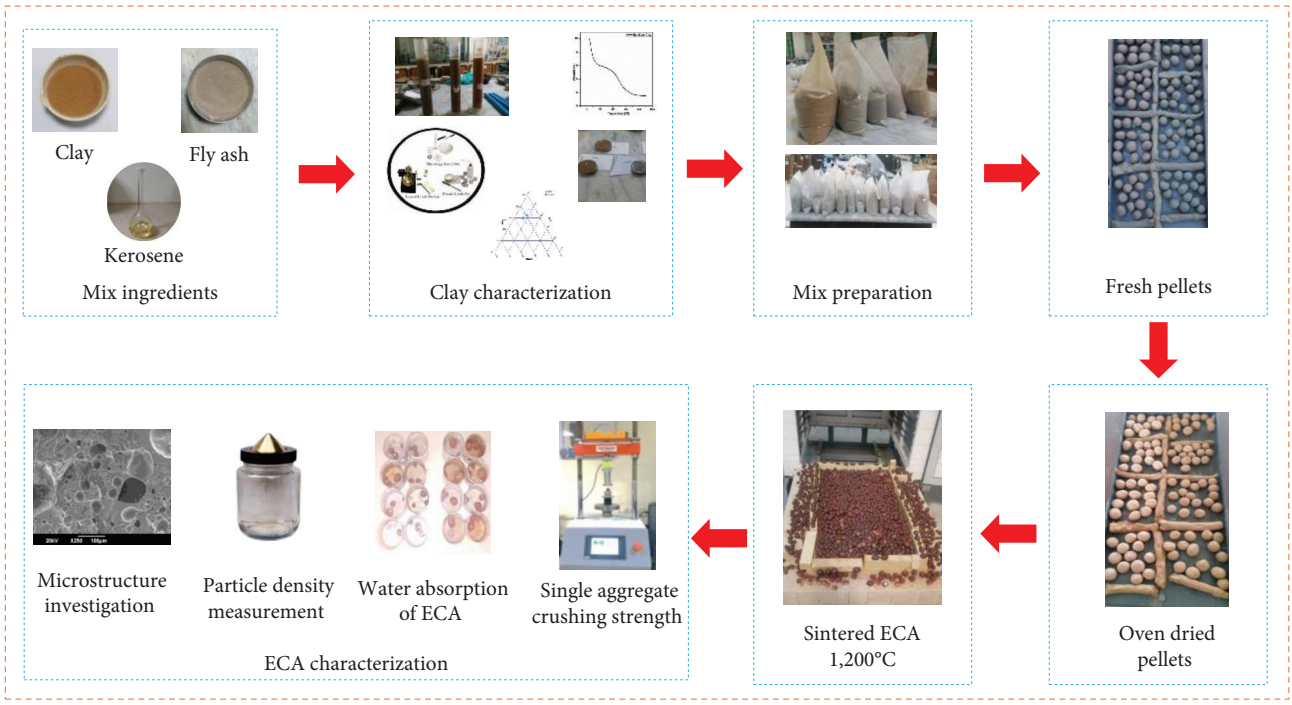

Figure 2: Schematic diagram showing the stepwise manufacturing scheme of ECA in the laboratory.

found using Equation (4). Apart from water, the amount of kerosene and fly ash was added as mentioned in the mix design. After finalizing the mix design and properly mixing the ingredients, pellets of size 15 mm were made by hand, and the size was ensured through a Vernier calliper. The pellet size was retained at 15 mm since the size change after calcination would be easily visible at this size. The primary challenge with pelletization is controlling aggregate size. On a lab scale, the size was ensured by a Vernier calliper because of the fewer number of pellets. Twenty-five pellets of each mix design were prepared to assure accuracy and reduce the possibility of mistakes. After drying the pellets in the oven for 48 hr at 110°C, they were shifted to the kiln and sintered at a temperature ranging between 1,100 and 1,300°C keeping in consideration the results of thermogravimetric analysis (TGA) of the clay and fly ash discussed in the later sections of the article in article. Figure 2 depicts a visual description of the steps performed in the laboratory to form ECA. The rate of temperature increment was kept 20°C/min initially and later on increased in accordance to the previous investigation on high plastic clay by Lo et al. [37], and the overall temperature profile follows the previous investigation on the same clay by Hussain et al. [36] shown in Figure 3.

Following aggregate synthesis, a complete characterization was carried out to investigate aggregates' physical and chemical characteristics. First, their water absorption was measured by submerging them in water for 24 hr. To track the mass loss as the temperature rose over time, a thermogravimetric study was done and to find the composition of aggregate, energy dispersive X-ray spectroscopy (EDX) was performed [25]. The crushing strength of aggregate and bulk density were also evaluated to find their appropriateness for

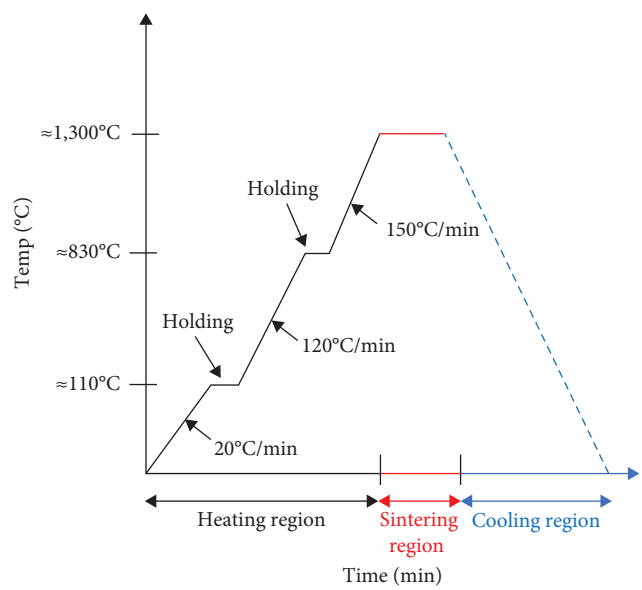

Figure 3: Temperature profile implemented for ECA synthesis [36].

lightweight concrete. And lastly, a SEM was used to examine the aggregate's morphology at various fly ash and kerosene dosages.

2.4. Mix Design and Casting of Lightweight Aggregate Concrete (LWAC). After the synthesis of ECA from clay, an investigation was conducted to evaluate their potential use in LWAC. The purpose of this investigation is to decipher the feasibility of this concrete in the manufacturing of lightweight non-structural concrete masonry. The core constituents used for

Table 3: Trial mix design of lightweight aggregate concrete.

S. no	Mix name	Cement (% of binder)	Fly ash (% of binder)	*W*/*B* (% of binder)	ECA (Kg/m^3)	Binder (Kg/m^3)
1.	Mix-A1	70	30	0.5	380	300
2.	Mix-A2	50	50	0.5	380	300
3.	Mix-A3	30	70	0.5	380	300
4.	Mix-B1	70	30	0.55	380	300
5.	Mix-B2	50	50	0.55	380	300
6.	Mix-B3	30	70	0.55	380	300

Table 4: Physical properties of CFK-2 aggregate used in the development of lightweight aggregate concrete.

Physical property	Value
Loose bulk density (g/m^3)	0.59
Compressive strength of single aggregate (MPa)	0.82
Water absorption (%)	11.50
Loss on ignition (%)	24.32
Bloating index (%)	33.33

the concrete casting include ECA, cement, fly ash, and water (Table 3). The selection of the recipe CFK-2, was predicated upon its exceptional properties, extensively elaborated upon in subsequent sections of this article and comprehensively detailed in Table 4. A trio of precisely tailored mix designs was conceptualized, entailing incremental substitutions of fly ash for cement at weight proportions of 30%, 50%, and 70%. The *W*/*B* ratio was kept 0.5 and 0.55 keeping in view the instructions by Leca® International, a leading company in the field of ECA (Table 3). Rodrigues and Bragança [8] also concluded that the compressive strength of LWAC was optimum at *W*/*B* of 0.5.

LWAC casting process is usually cumbersome because if the ingredients are mixed conventionally in a mixer, and then poured into the mold, the aggregates float on the surface, resulting in uneven distribution of aggregates within the matrix [38, 39]. Preplaced aggregate concrete (ASTM C-937 [40]) is a new method for casting LWAC in which aggregate is first placed in a mold then the mortar is added to the mold [38]. Therefore, this approach was undertaken in which the aggregates were initially placed in the concrete cubes and adequately compacted. Then, the mortar was prepared in a Hobart mixer according to the proposed mix design and poured into the mold. After casting, the samples were cured for 28 days before testing. Figure 4 represents the two-stage casting method. After the casting and curing of concrete samples, their mechanical properties, i.e., density, compressive strengths, pullout strengths, flexural strength, ultrasonic pulse velocity, and split tensile strength of concrete were found were found by performing their standardized tests. Also, an in-depth study of the microstructure and elemental composition of the optimum mix was also carried out.

3. Results and Discussion

3.1. Characterization of Clay. It is evident from the particle size distribution curve that clay does not contain any sand content and when the sand fraction and Atterberg limits were interpolated on the newly proposed texture-based classification and plasticity-based classification of clays. It was found that clay fell in pure clay texture region and clay-low compressibility plasticity region as shown in Figure 5. Although high plastic clays are well-suited for ECA pelletization due to their higher water retention and ease of pelletization, usually they are not recommended for general construction purposes because of their susceptibility to settlement issues. Table 5 shows the fundamental geotechnical properties of the clay under study.

When clay particles are analyzed through laser particle size analyzer S3500 Microtrac, it was found that this specific clay has lower a particle size than typical clay samples. The clay's surface area increases significantly because of the particle size reduction, which increases its capacity to retain water molecules inside its porous structure. As a result, when exposed to high temperatures, the clay's stored water tries to escape, resulting in increased bloating phenomenon. The clay particle distribution of clay after passing through the #200 sieve is shown in Figure 6.

The TGA results in Figure 7 indicated that the major loss of mass of fly ash and clay is in between 50 and 900°C. Therefore, the bloating temperature range of 1,100–1,200°C was enough for adequate bloating within the aggregates. The flattening observed at the curve at 200°C is due to the dehydroxylation of the minerals within clay while the flattening at 600°C is due to the low to high polymorphic transformation of quartz minerals [42].

Before sintering, the raw clay and fly ash were subjected to XRD and XRF analysis to find their minerology band elemental composition. The XRD analysis confirmed the presence of montmorillonite in the clay (Figure 8), that is a smectite type element and indicates the high bloatability of the clay. Montmorillonite is known for its interlayer water storage capacity and this stored water tries to escape upon heating which results in the bloating of ECA [43]. Montmorillonite 's increased cation exchange capacity is also another reason for its increased bloatability. The XRF analysis, as shown in Table 6, also verifies the presence of interlayer cations such as Na^+, Mg^{+2}, K^+, and Ca^{+2}, indicated as Na_2O, MgO, K_2O, and CaO, respectively. Likewise, the previous studies, the XRD analysis also confirms the presence of quartz, although it is very thermally stable and does not participate significantly in the bloating.

The results of the XRF analysis were used to find the SiO_2/flux index of clay. The SiO_2/flux index of clay plays a

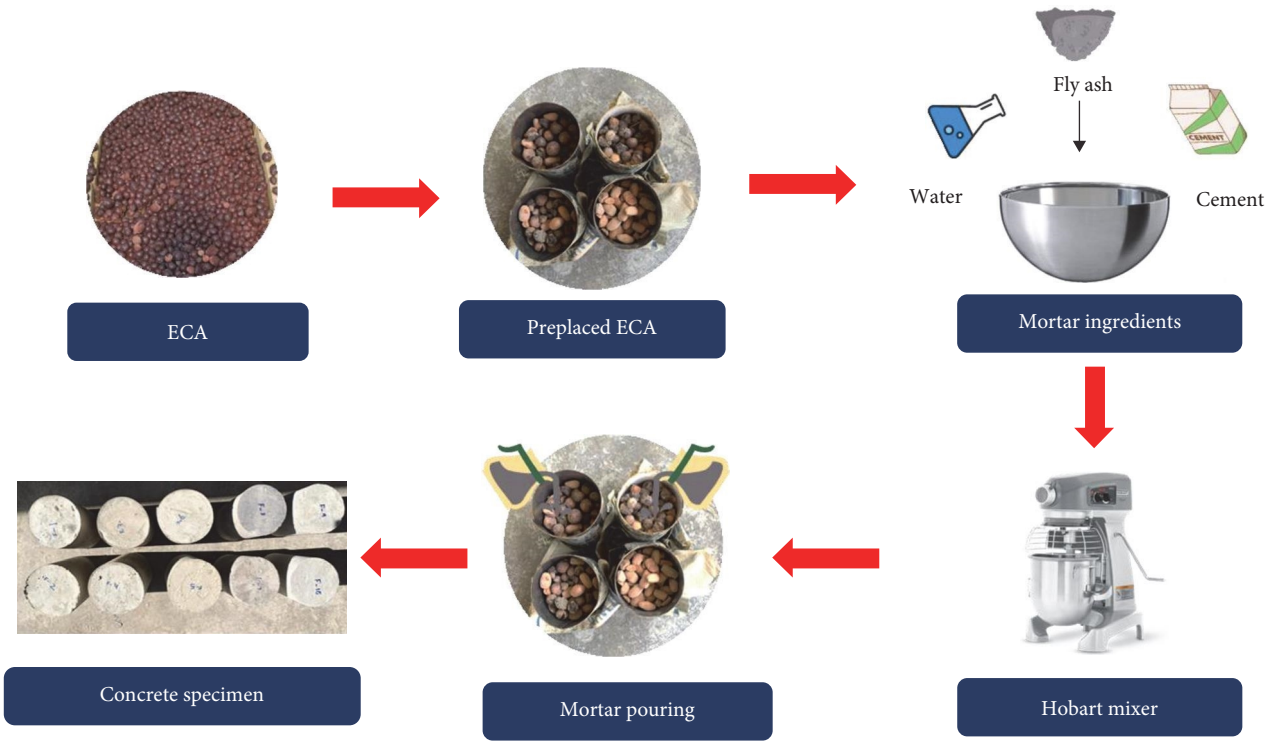

Figure 4: Schematic diagram showing the stepwise procedure casting of preplaced LWAC.

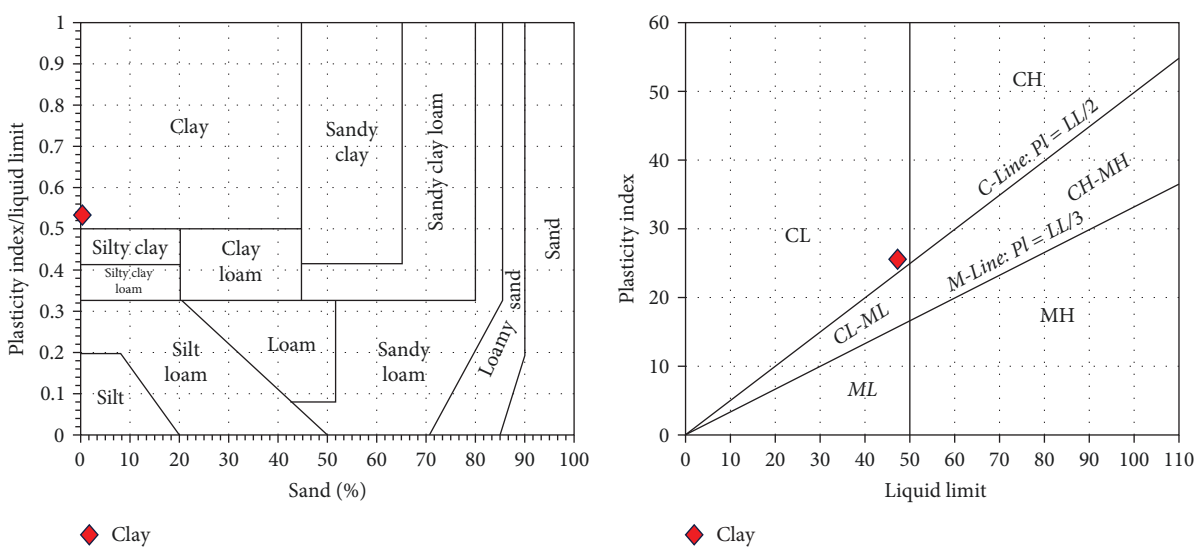

Figure 5: Depiction of clay types in the diagrams developed by Moreno-Maroto and Alonso-Azcárate [41]: (a) liquid limit (LL) and plasticity index (PI) based plasticity chart and (b) sand particle fraction and the ratio of plasticity index (PI) to liquid limit (LL) based textural chart. Symbols in this chart correspond to different characteristics; C represents clay, M stands for silt, L indicates low compressibility, and H denotes high compressibility.

Table 5: Atterberg limits of clay (%).

Clay name	Liquid limit	Plastic limit	Plasticity index	Shrinkage limit	Maximum toughness (T_{max})	Optimal moisture content
Nandipur	48.6	23.90	24.70	8.19	22	29.5

SL = shrinkage limit, LL = liquid limit, PI = plastic index, and PL = plastic limit.

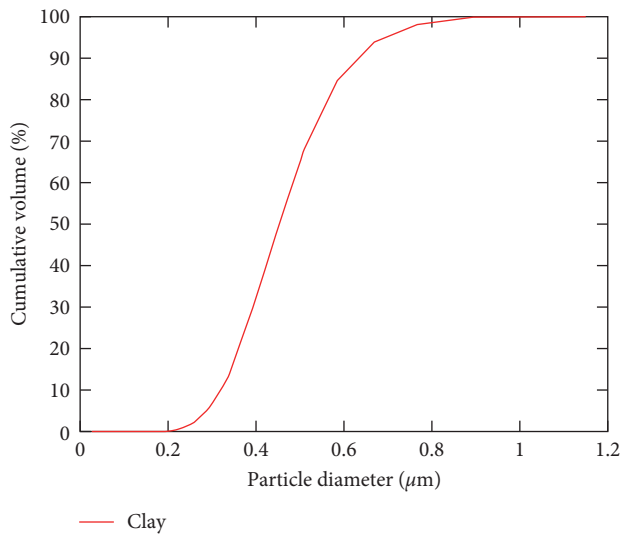

Figure 6: Laser particle size distribution of the clay.

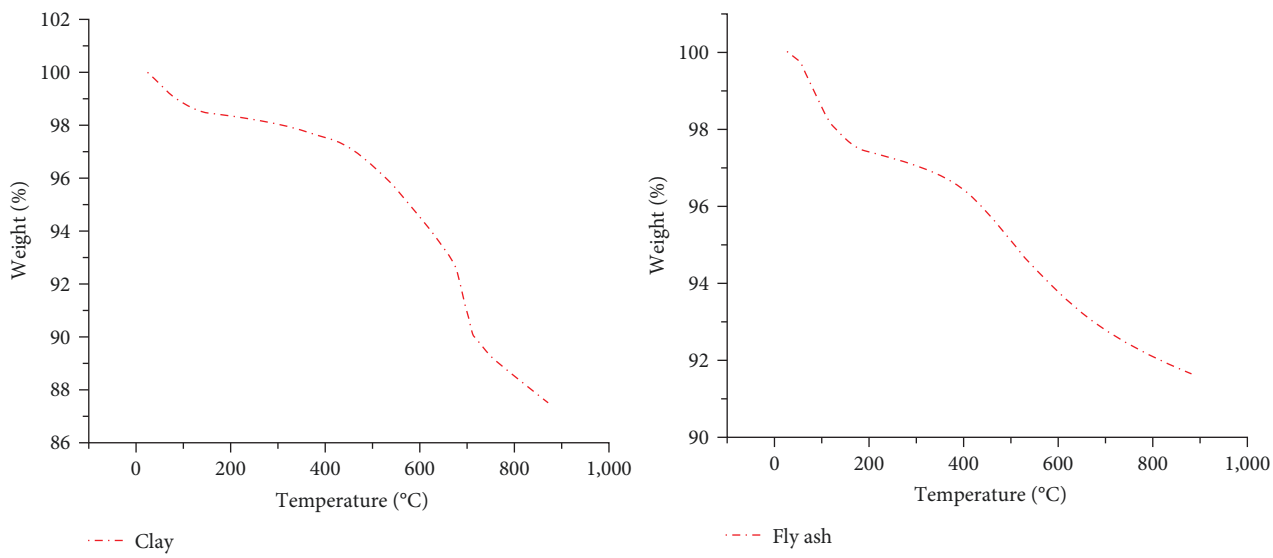

Figure 7: Results of thermogravimetric analysis of clay indicates the temperature range of mass loss.

pivotal role in determining the potential for bloating in clay materials. This essential parameter is established by dividing the silica (SiO_2) content within the clay by the concentration of fluxing agents, such as calcium oxide (CaO) and magnesium oxide (MgO). Clays with higher SiO_2/flux index tend to bloat at a lower temperature while those with lower SiO_2/flux index require higher bloating temperatures. Also clays with higher SiO_2/flux index bloat more than those with SiO_2/flux index if given the same bloating temperature [37]. The SiO_2/flux ratio of clay came out to be 3.98, positioning it within the high bloating spectrum. Furthermore, the chemical composition of the clay showcases noteworthy levels of SiO_2 and Fe_2O_3. Visualization of the chemical composition using Riley's diagram indicates the clay's categorization within the bloating range, as identified by Riley [32], as depicted in Figure 9.

3.2. Expanded Clay Aggregate

3.2.1. Color, Morphology, and Microstructure. When comparing an average ECA of PC, CF, CK, and CFK, all four types of aggregates have a dominating brick-red hue with a tan or dark grayish undertone. The CF1, CF2, and CF3 ECAs, however, were darker due to a slightly higher fly ash content while the CK1, CK2, CFK1, and CFK2 recipes had shinier surfaces. As far as the surface textures are concerned, PC aggregates were characterized by smooth surface textures, followed by CF and CK, which had somehow more uneven surface textures, and CFK, which had the most irregular and rough textures, as indicated by Figure 10. This is probably due to the increased bloating of CFK aggregates as compared to other recipes.

After characterization and sintering of clay, the aggregates were ready for further investigations. A SEM FEI Magellan

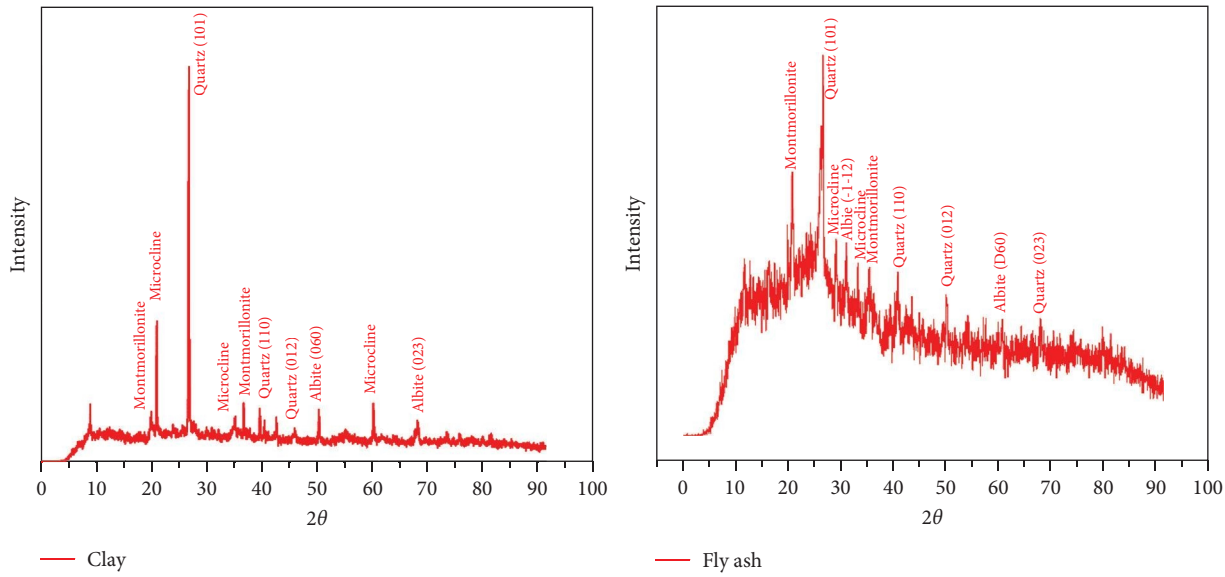

Figure 8: XRD analysis of clay and fly ash.

Table 6: XRF analysis of clay and fly ash.

Sample name	Chemical composition									
	SiO_2	Al_20_3	Fe_2O_3+FeO[a]	Na_2O[a]	K_2O[a]	MgO[a]	CaO[a]	TiO_2	SO_3	$SiO_2/\sum Flux$
Clay	58.57	17.69	6.90	0.56	3.04	2.88	1.32	0.81	0.00	3.98
Fly ash	51.53	22.43	8.84	0.23	0.39	3.18	4.84	1.62	2.75	2.95

[a]Fluxing oxides.

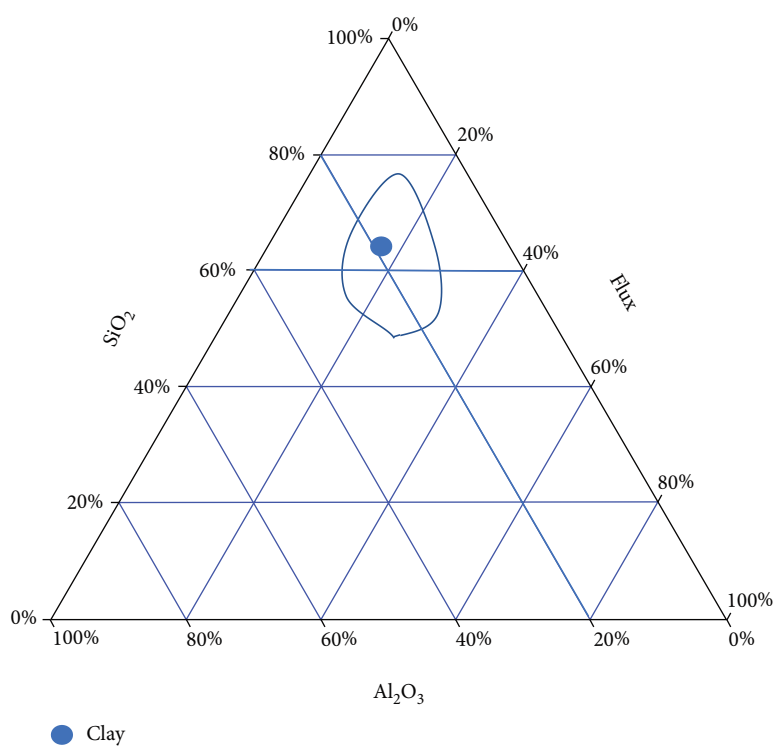

Figure 9: Interpolation of clay in the bloating zone of Riley [32] diagram.

Original pellet size	PC	CF1	CF2	CF3
15 mm	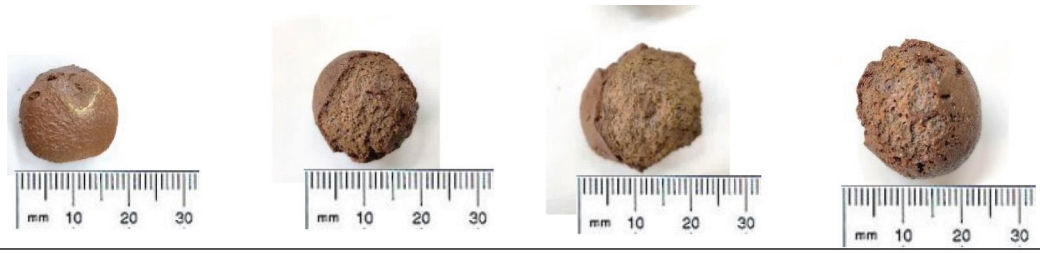			
Original pellet size	CK1	CK2	CFK1	CFK2
15 mm				

Figure 10: Pictures comparing the morphologies and textures of all the mix recipes.

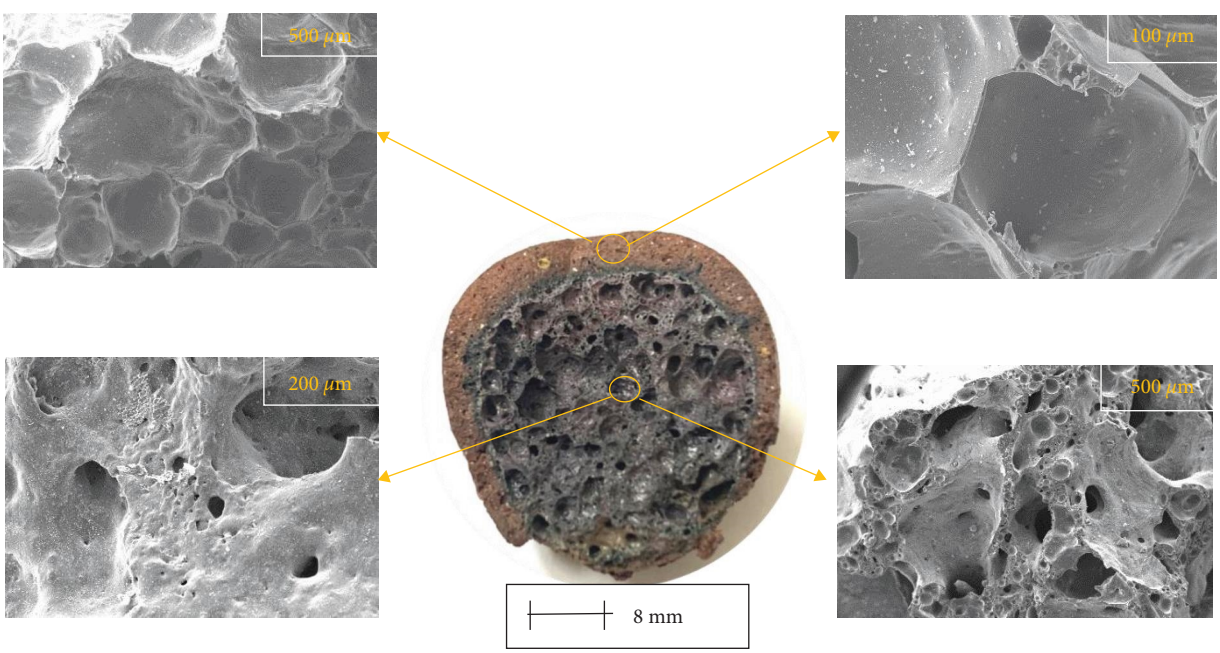

Figure 11: SEM imagery to explore the internal core and exterior shell of ECA.

400, with a magnification range of 300,000x high-end, was utilized to examine the microstructure of CFK2 aggregate recipe which had the highest amount of kerosene and fly ash. Three different magnification factors were used to view the interior microporous structure of aggregate. The SEM results indicate that the internal structure was composed of interconnected pores and channels that provide a large surface area for air and water exchange [37]. The outer covering

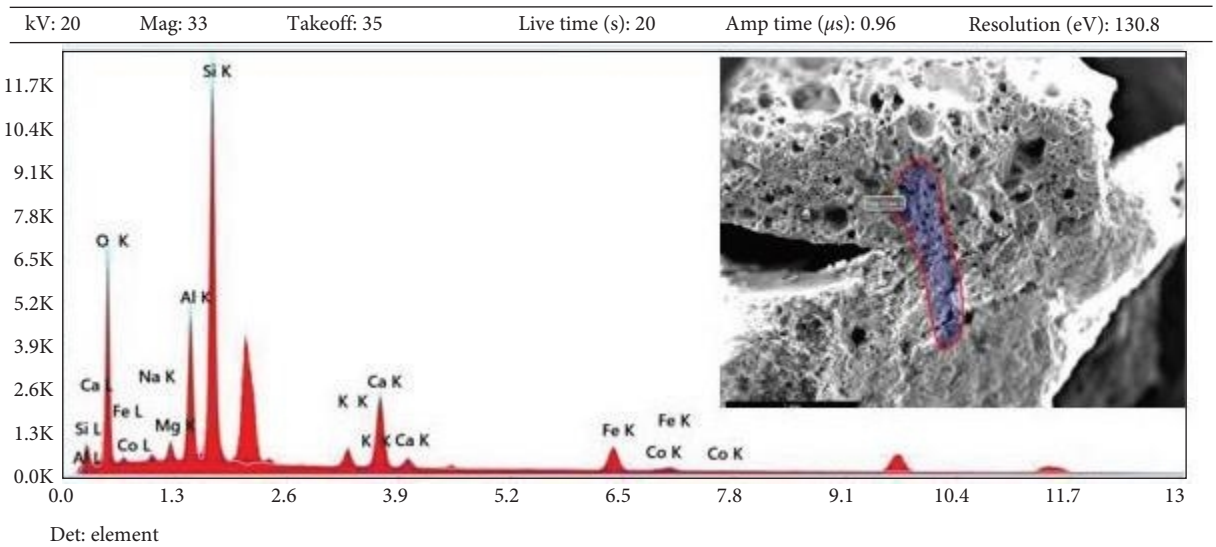

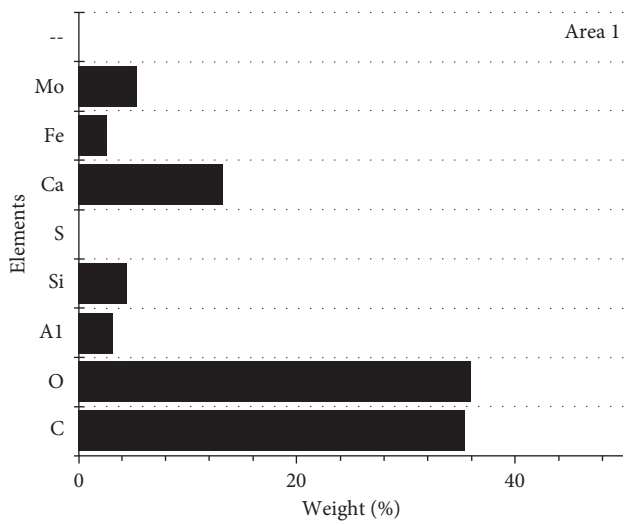

(a)

Figure 12: Continued.

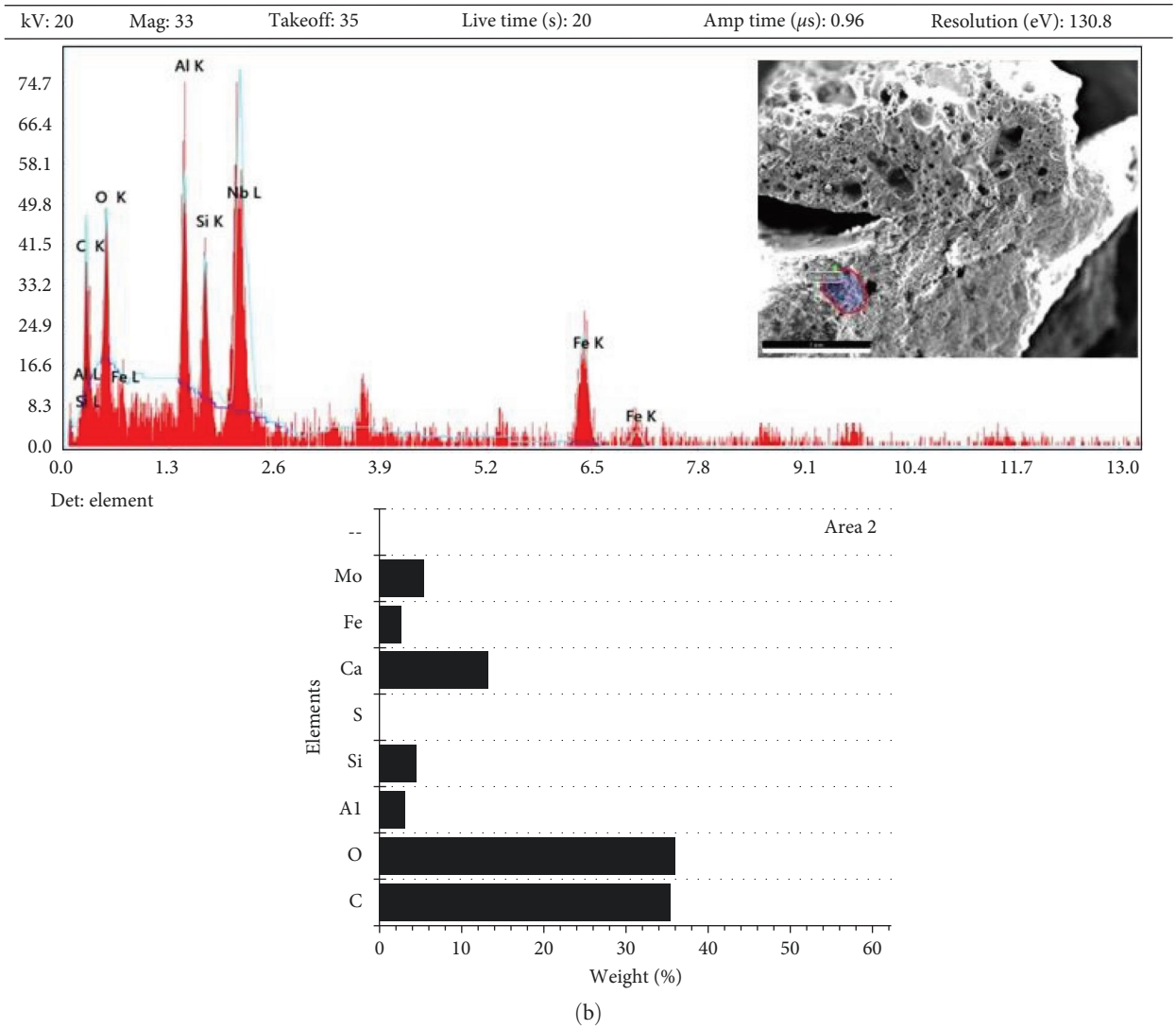

(b)

Figure 12: EDX analysis of CFK2 ECA: (a) area 1 of CFK2 recipe and (b) area 2 of CFK2 recipe.

of ECA had a dense microstructure with clay particles visible in the SEM images and the inner core of ECA was further separated into two layers: the outercore layer, which had smaller pores, and the innercore, which was characterized by large, irregular pores as shown in Figure 11.

The elemental composition analysis of CFK2 aggregate, as depicted in Figure 12 through EDX spectroscopy, reveals the presence of Si, O, and Al, aligning with the findings in Table 6 for clay from XRF analysis, as corroborated by Shokri [44] in their research on ECA.

3.2.2. Bloating Index and Loss on Ignition. The loss of ignition (LOI) and bloating index (BI) are the key parameters to analyze the extent of bloating of ECA. LOI is used to quantify mass loss due to the removal of volatile and organic content while bloating index quantifies the volumetric expansion of ECA on exposure to temperature [36]. BI and LOI were found using Equations (5) and (6). Figure 13 compares the LOI and BI of mix recipes of ECA used in this study.

$$\mathrm{LOI} = (w_i - w_f)/w_i, \tag{5}$$

$$\mathrm{BI} = [(d_2 - d_1)/d_1] \times 100. \tag{6}$$

3.2.3. Density. ASTM C-29 [45] was employed for finding the bulk density of aggregates. As previously stated, the CFK-2 ECAs inflated the most, resulting in the lightest aggregates with a bulk density of 0.53 g/cm^3. The porous nature of CFK-2 aggregate explains why this aggregate is the lightest. The bulk shows the average densities of the four categories of ECAs studied in this article. EN-13055-1 indicates that aggregates having a density of <2 g/cm^3 are considered LWAs and all the aggregates fall in the lightweight category [46]. Table 7 shows the average densities, water absorption, compressive strength, and single aggregate to particle density (S/ρ_A) values of all ECA mixes used and all the values are in accordance with the standards for LWAC masonry.

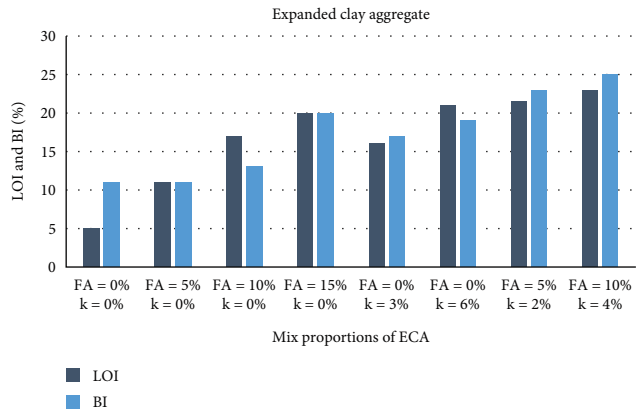

FIGURE 13: Loss on ignition and bloating index of ECA mix recipes.

TABLE 7: Physio–mechanical characterization of ECA.

Clay sample	Nandipur clay-1,200°C				
	PS	ρ_A	WA_{24}	S	S/ρ_A
PC	15	0.88	6.91	1.73	1.97
CF1	15	0.83	8.62	1.68	2.02
CF2	15	0.66	6.13	1.85	2.80
CK3	15	0.60	9.34	1.12	1.87
CK1	15	0.61	9.5	1.07	1.78
CK2	15	0.53	10.50	1.08	2.03
CFK1	15	0.60	11.12	0.84	1.40
CFK2	15	0.59	11.15	0.82	1.38

S = crushing strength of single aggregate (MPa), ρ_A = particle density (g/cm^3), WA_{24} = water absorption (%), PS = pellet diameter (mm), and S/ρ_A = single aggregate crushing strength to particle density.

3.2.4. Compressive Strength. The compressive strength and density of aggregates are usually directly proportional. The aggregates that have hollow internal structures are lighter and have less crushing strength. And those aggregates which have more dense and compact internal structures have been stronger in compression. From a concrete point of view, an aggregate must be lightweight as well as should have adequate strength and the balance between these two parameter of density and crushing strength has given rise to the coefficient of S/ρ_A, for LWAs [47]. S/ρ_A value is the ratio of crushing strength and particle density of aggregates. de Gennaro et al. [48] reported that aggregates of $S/\rho_A > 3.46$ can be used in structural concrete and none of the aggregate recipes studied in this research qualified that threshold.

3.2.5. Water Absorption. The water absorption of ECA was measured according to ASTM C127M [49]. According to the results indicated in Table 7 aggregates of CFK-2 had a water absorption of 11.15%, greater than other recipes. This is probably due to the increased and continuous porosity of CFK-2 aggregates as compared to other mix recipes. The pores within the internal structure of ECA act as reservoirs for water and increased porosity provides increased surface area for the water to be retained. Also, the continuous porosity of CFK−2 aggregates results in capillary action of water which is also a reason for higher water absorption.

3.3. Lightweight Aggregate Concrete (LWAC)

3.3.1. Compressive Strength of LWAC. After the curing of concrete cylinders with 200 mm height and 100 mm diameter, they were tested according to ASTM C-39 [50]. Table 8 presents the mechanical properties of LWAC, while Figure 14 illustrates the testing configurations employed for evaluating LWAC. Mix A1 which had 70% cement and 30% fly ash as binder had the highest compressive strength of 14 MPa and on the lower end, Mix B3 with 30% cement and 70% fly ash as a binder reached 6.8 MPa. According to ASTM C-129 standards, the minimum strength for structural concrete is 17 MPa and that for nonstructural members is 3.45 MPa [51]. Therefore, the LWAC made from ECA satisfied the criterion for nonstructural concrete. According to Abrams Law [52], there exists an inverse relationship between the water-to-cement (w/c) ratio and the compressive strength of concrete. For instance, when the w/c ratio is 0.40, the concrete achieves a compressive strength of 34 MPa. Conversely, if the w/c ratio is increased to 0.50, the compressive strength decreases to 21 MPa. Fernando et al. [53] did a detailed experimentation on expanded polystyrene-based infill panels for nonload bearing masonry and found that it has maximum compressive strength of 2.89 MPa however comparatively, all the mixes studied in this research qualify this threshold.

3.3.2. Density of LWAC. After compressive strength, the density of the LWAC was found according to ASTM C-138 [54]. As expected, Mix A1 had the highest density of 1,149 kg/m^3 and Mix B3 had the lowest density of 1,050 kg/m ^{3}. This is because fly ash has a density of nearly half of that cement and the mix with more cement as a binder. Mix A1 and Mix B1 turned out to be denser than other mixes since they had comparatively less fly ash as a replacement of binder. Conventional normal-weight concrete has a density of up to 2,400 kg/m ^{3}. Consequently, Mix B3, the lightest composition, exhibits a remarkable 55% reduction in density compared to typical normal-weight concrete. This substantial reduction holds the potential for significant cost savings in steel, particularly when this LWAC is used as infill material [55]. According to EN-1992, the density of lightweight concrete must lie between 800 and 2,000 kg/m^3 and the concrete mixes of this study comply with this standard [56]. Also, the density of all the mixes complies with the standards for concrete masonry ASTM C-55 [51] and ASTM C 129-11 [51] of nonloadbearing concrete masonry units.

3.3.3. Pull-Out Strength of LWAC. In our study, we rigorously assessed pull-out strength, adhering to ASTM C 900-15 standards [57]. Cube-shaped 100 mm^3 specimens were meticulously cast and cured for 28 days. A metal insert was securely embedded in the concrete during initial casting. To measure in-place pull-out strength, a hydraulic jack applied force to the insert against a robust bearing ring until failure, with the maximum force recorded.

Table 8: Mechanical properties of LWAC.

Sr. no	Mix name	Density (kg/m^3)	Compressive strength (MPa)	Split tensile strength (MPa)	Ultrasonic pulse velocity (m/s)	Pull out strength (MPa)	Flexural strength (MPa)
1.	Mix-A1	1,149	14	1.5	4.9	2.5	0.8
2.	Mix-A2	1,106	9	0.8	4.2	1.63	0.65
3.	Mix-A3	1,090	7.1	0.68	3.9	1.25	0.62
4.	Mix-B1	1,130	12.5	1.3	4.5	2.11	0.73
5.	Mix-B2	1,101	10	0.9	3.6	1.1	0.68
6.	Mix-B3	1,050	6.8	0.6	3.2	0.89	0.6

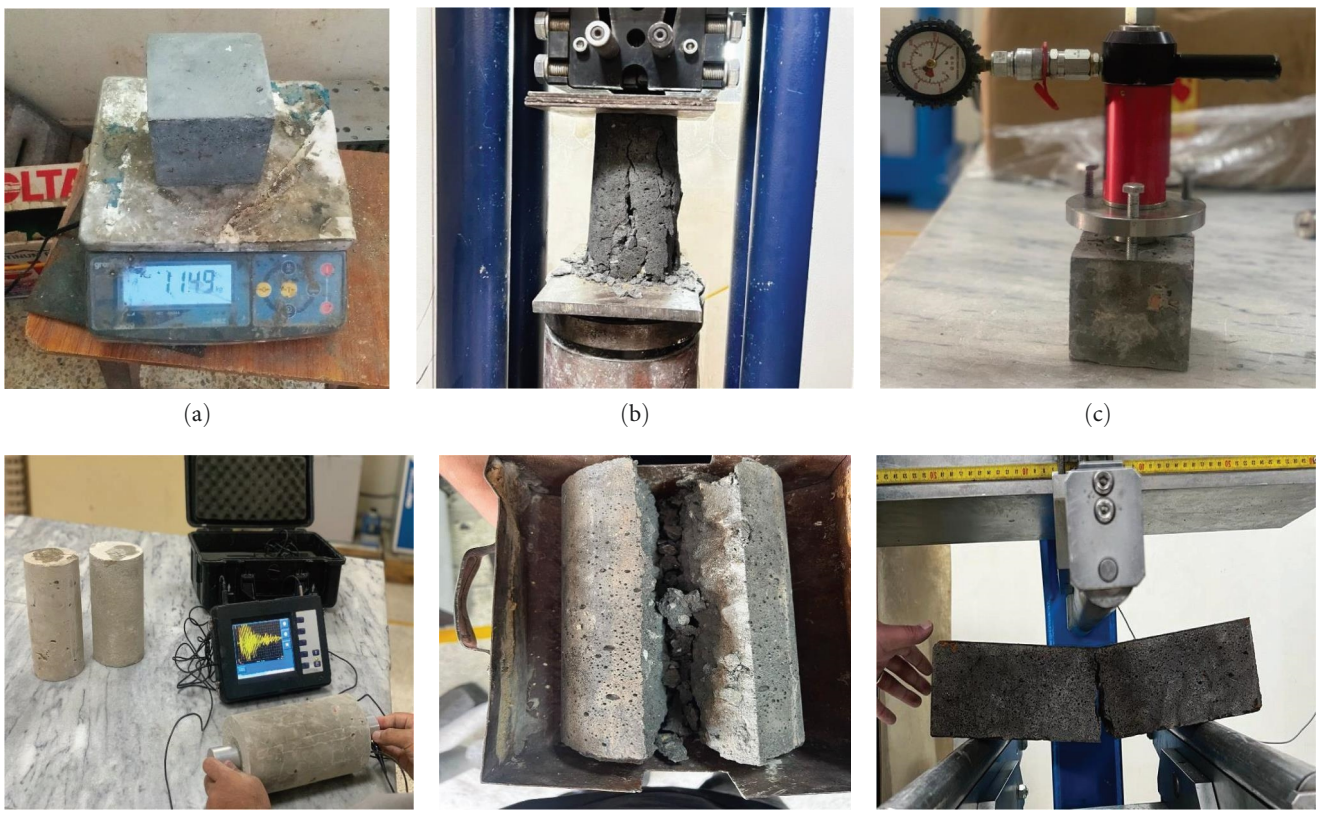

(a) (b) (c)

(d) (e) (f)

Figure 14: Mechanical properties of LWAC: (a) density, (b) compressive strength, (c) pull-out strength, (d) UPV, (e) split tensile strength, and (f) flexural strength.

Mix A1 exhibited the highest pull-out strength of 2.5 MPa. Conversely, as fly ash content increased, Mix A2 and Mix A3 showed reduced 28-day strength. Higher *w*/*c* ratios led to decreased pull-out strength, with Mix B3 recording the lowest at 0.89 MPa. Similar trends have been found by Bogas et al. [58] in his investigations of up to 40% replacement of cement with fly ash.

3.3.4. Ultrasonic Pulse Velocity of LWAC. In this comprehensive study, the ultrasonic pulse velocity (UPV) test was executed in strict accordance with ASTM C 597-16 standards [59]. Cylinder-shaped specimens, measuring 200 mm in height and 100 mm in diameter, underwent a 28-day curing process under controlled environmental conditions. Utilizing TMC-3850, ultrasonic pulses were transmitted through the concrete specimens, and precise travel times from source to receiver were measured.

Mix A1 resulted in the highest UPV of 4.3 km/s and with the increase in fly ash content, the 28 days strength decreased, in Mix A2 and Mix A3. Increased cement content leads to a stiffer and denser concrete, resulting in faster wave propagation and a higher UPV [60]. Increase in *w*/*c* resulted in decrease in UPV and the sample Mix B3 had the lowest UPV of 2.9 km/s. This is because excess water in the mix increases the porosity of the concrete and creates more obstacles for the ultrasonic waves to travel through [61].

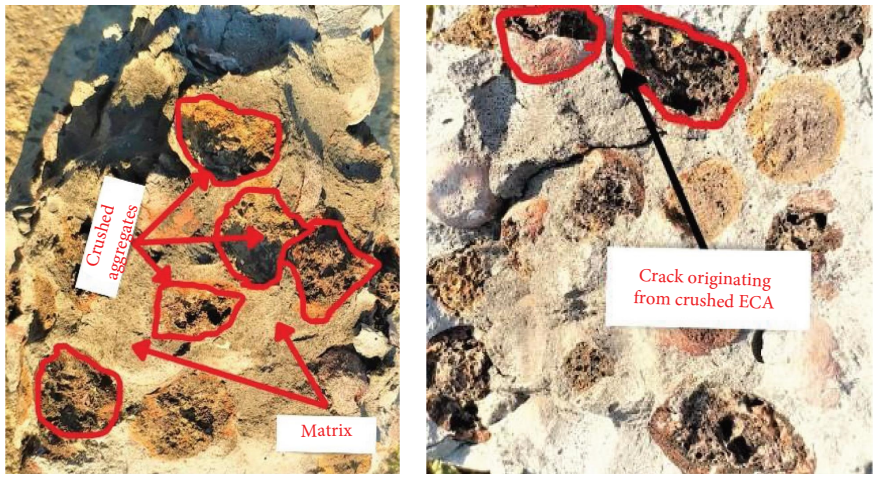

(a) (b)

Figure 15: Failure surface of LWAC: (a) crushed aggregates and (b) crack initiation in concrete.

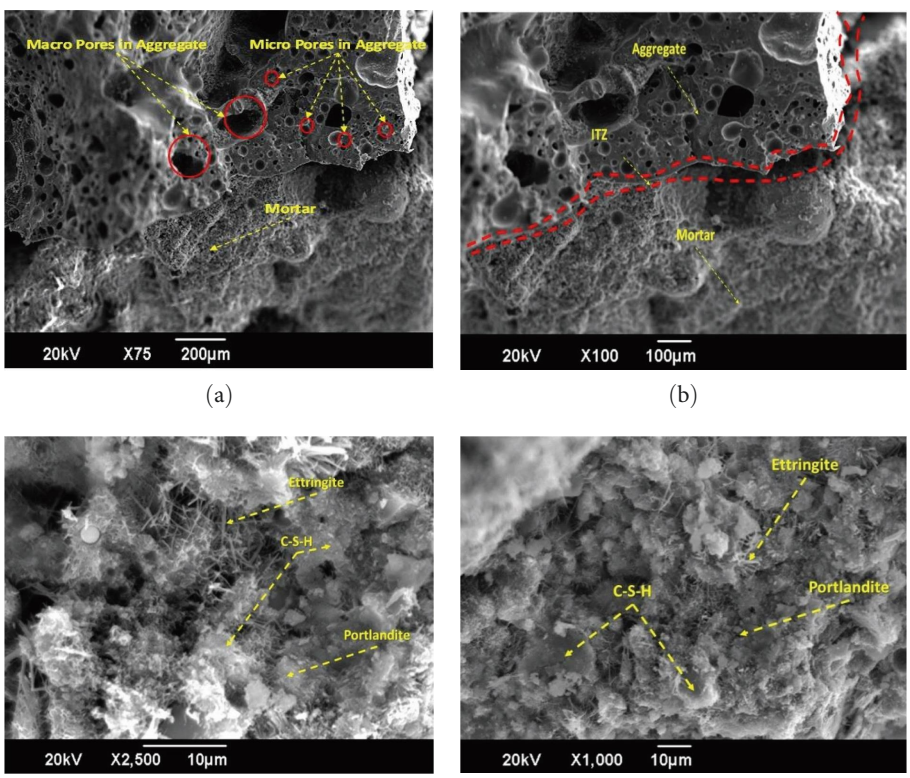

(a) (b)

(c) (d)

Figure 16: (a) SEM image of concrete showing ECA microstructure and porosity, (b) SEM image of concrete showing ITZ and (c, d) SEM image of concrete matrix.

Concrete with UPV < 3 km/s is considered poor, so all the mixes do not fall in that region. However, only Mix A1 and Mix B1 are the only mixes with UPV > 4.4 km/s and fall in the excellent category.

3.3.5. Split Tensile Strength of LWAC. The split tensile strength test adhered ASTM C496/C496M-17 [62]. Cylinder-shaped specimens, measuring 200 mm in height and 100 mm in diameter, were meticulously prepared and subjected to a precise 28-day curing process in controlled environmental conditions. During testing, the specimens were centered on the upper bearing block and ensured that the diametral line projections were aligned with the upper and lower bearing plates. Then load was applied according to the standards and finally split tensile strength was found by putting the failure load in the formula below.

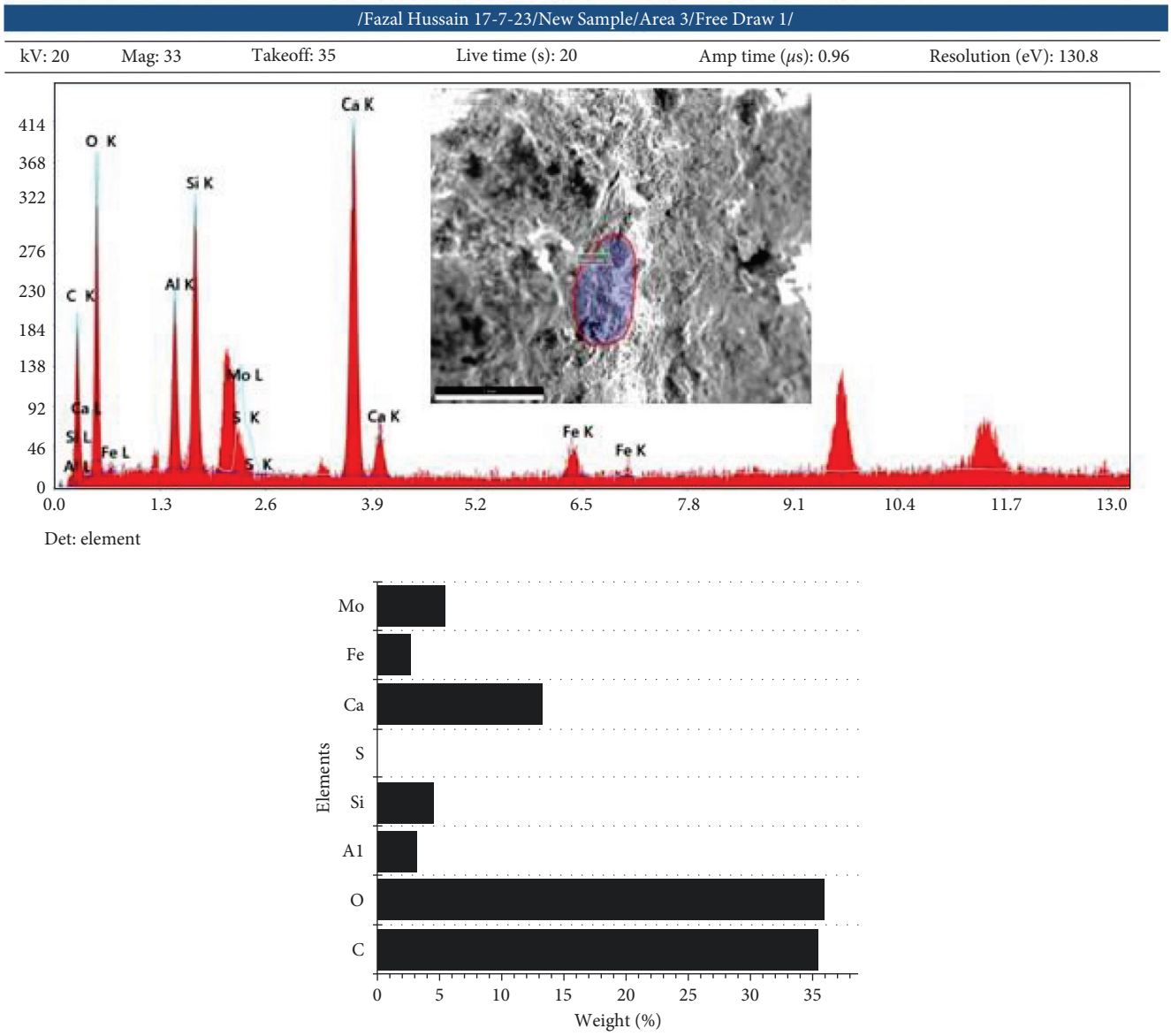

Figure 17: EDX spectrsocopy of concrete matrix.

$$T = \frac{2P}{\pi LD}. \tag{7}$$

T = tensile strength, P = failure load, L = length of specimen, and D = diameter of specimen.

Mix A1 resulted with the highest split tensile strength of 1.5 MPa and with the increase in flyash content, the 28 days strength decreased, in Mix A2 and Mix A3. Increase in w/c ratio resulted in decrease in split tensile strength and the sample Mix B3 had the lowest split tensile strength of 0.6 MPa. Although the samples with higher fly ash percentages have lower 28 days strength but they will have better physio–mechanical properties in the long run.

3.3.6. Flexural Strength of LWAC. The assessment of flexural strength adhered to ASTM C293M [63]. Prismatic specimens, characterized by dimensions of $100 \times 100 \times 400$ mm, were meticulously prepared and subjected to a precisely controlled 28-day curing process in environmentally regulated conditions. During the testing process, the specimens were carefully positioned on the flexural testing apparatus, ensuring proper alignment and support. The flexural strength was then found according to the formula below.

$$T = \frac{3PL}{2BD^2}. \tag{8}$$

R = rupture modulus, P = failure load, L = length of span, B = specimen width, and D = depth of specimen

Mix A1 exhibited the highest flexural strength of 0.8 MPa. Conversely, as fly ash content increased, Mix A2 and Mix A3 showed reduced 28-day strength. Higher w/c

ratios led to decreased split flexural strength, with Mix B3 recording the lowest of 0.6 MPa. Fernando et al. [53] did a detailed experimentation on expanded polystyrene-based infill panels for nonload bearing masonry and found that it has maximum flexural strength of 0.31 MPa and all the mixes studied in this article qualify this threshold.

4. Failure Mechanism and Microstructure of LWAC

In conventional normal-weight concrete, failure typically initiates at the interface of the aggregate–concrete bond known as ITZ (interfacial transition zone). This failure then progresses into the matrix and propagates [64]. On the contrary, lightweight concrete experiences a different failure pattern, where the aggregates themselves are the vulnerable component, and failure initiates through the crushing of these aggregates [65]. As a result, the behavior of normal-weight concrete upon failure is ductile due to the gradual propagation of cracks from the ITZ into the matrix, and further from one aggregate's ITZ to another. This transition takes time, contributing to the material's ductile response [66]. Conversely, LWAC exhibits brittle failure tendencies. The failure of LWAC involves the rapid bursting or crushing of aggregates, rendering it more brittle in comparison to normal-weight concrete [8]. Figure 15(a) depicts the aggregate failure of the LWAC where the distinctive dark internal core of the ECA is easily discernible and Figure 15(b) indicates the origination of crack from crushed aggregate.

The SEM imagery of Mix A1's cross-section provides a comprehensive view of its intricate composition, featuring the porous ECA, the compact mortar matrix, and the crucial ITZ where aggregate and concrete converge Figures 16(a) and 16(b). Upon closer examination at higher magnifications, a fascinating level of detail emerges. Notably, the micrograph reveals the presence of ettringite, presenting itself as well-defined crystalline structures. In addition, the calcium silicate hydrate (CSH) gel showcases its distinct morphological diversity, with some regions appearing fibrous while others exhibit a more platy or granular character. The well-developed CSH matrix enhances the structural integrity of the concrete by providing strength and reducing permeability, crucial for long-term performance [64]. Lastly, the image highlights the form and distribution of portlandite crystals, shedding light on their potential impact on concrete's long-term performance and durability Figures 16(c) and 16(d).

The EDX analysis of the concrete matrix Figure 17 revealed notable percentages of carbon, oxygen, and calcium. The presence of higher carbon levels indicates deliberate inclusion of fly ash within the concrete mix. This strategic utilization of fly ash serves to enhance sustainability efforts while mitigating heat generation during the curing process, aligning with modern construction practices. Mix A3 and Mix B3 exhibit remarkable fly ash incorporation, accommodating up to 320 kg of fly ash in 1 m^3 of concrete. Increased oxygen levels, a common feature in concrete, is due to the dominant presence of critical phases like CSH and portlandite in the concrete.

5. Conclusion

This research project focused on investigating a distinctive ECA mix design, which involved the incorporation of fly ash and kerosene with clay. The central objective was to create environmentally sustainable nonstructural concrete utilizing ECA. After successfully synthesizing sustainable and lightweight ECA, the study explored their potential application in LWAC for nonstructural concrete for infills.

(i) CFK-2 mix has yielded with a density of 0.59 g/cm³, compressive strength of 0.82 MPa, water absorption of 11.15%, LOI and BI of 24% and 25% correspondingly and all the physical properties of the ECA used in LWAC production adhere to the standards outlined in ASTM C-331 for LWA.

(ii) The maximum compressive strength of 14 MPa was recorded for Mix A1 which was less than the minimum requirement of 17 MPa for structural concrete, according to ACI 318. The minimum compressive strength of 6.8 MPa was recorded for Mix B3 which was larger than the minimum requirement of 3.45 MPa for nonstructural concrete, set by ASTM C-129. Hence, all the mixes qualify the criterion for nonstructural concrete.

(iii) A maximum density of 1,149 kg/m^3 was recorded for Mix A1 and a minimum density of 1,050 kg/m^3 was recorded for Mix B3, which is almost 45% of the density of an average normal. All the mix recipes comply with the standards of ASTM C-55 for concrete masonry and ASTM C-29 for nonstructural masonry.

(iv) Mix A3 and Mix B3 exhibit the capacity to incorporate 320 kg of fly ash into 1 m³ of concrete, a significant benefit for nations with substantial fly ash production.

While the focus of this study is on Class C fly ash only, the use of Class F fly ash, bottom ash and other ash variations, presents avenues for valuable insights in future investigations. Since the focus of this study is developing lightweight nonstructural concrete and using these alternative compositions underscores potential areas for future research to expand this inquiry into lightweight structural concrete formulations. Moreover, the current study has not compared the samples cast with preplaced concrete with conventionally cast concrete in terms of mechanical performance, which if performed in future could enhance the comprehensive understanding of their performance and applicability.

Nomenclature

LWA: Lightweight aggregate
ECA: Expanded clay aggregate
XRF: X-ray fluorescence
XRD: X-ray diffraction
TGA: Thermogravimetric analysis
LL: Liquid limit

PL: Plastic limit
PI: Plasticity index
SL: Shrinkage limit
W_{op}: Optimal moisture content
SEM: Scanning electron microscopy
S: Compressive strength
ρ^{A}: Particle density
LOI: Loss on ignition
BI: Bloating Index.

Data Availability

All the data have been provided in the manuscript.

Conflicts of Interest

The authors declare that they have no known competing financial interests or personal relationships that could have appeared to influence the work reported in this paper.

Authors' Contributions

S.A.K, H.A, F.A, and F.H. contributed in the conceptualization. F.A, H.A, and S.A.K. contributed in the methodology. F.A, H.A, and R.A.K contributed in the validation. S.A.K and F.A contributed in the formal analysis. F.H. contributed in the investigation. H.A, F.A, F.H, and R.A.K. contributed in the resources. S.A.K, H.A, and F.H. contributed in the writing–original draft preparation. S.A.K and F.A. contributed in the writing–review and editing. F.A. contributed in the visualization. F.A and R.A.K contributed in the supervision. H.A, S.A.K, F.A, R.A.K, and F.H. contributed in the project administration. All authors have read and agreed to the published version of the manuscript.

Acknowledgments

This research work was totally supported by National University of Sciences and Technology (NUST), Sector H-12, Islamabad 44000, Pakistan. The authors would like to thank the staff of structures lab at NUST Institute of Civil Engineering (NICE), NUST, for allowing us to accomplish this work in their labs. Open access publishing facilitated by Western Sydney University, as part of the Wiley - Western Sydney University agreement via the Council of Australian University Librarians.

References

[1] ASTM C330, "Specification for lightweight aggregates for structural concrete," *ASTM International*, vol. 552, no. 18, Article ID 4, 2009.

[2] D. S. Vijayan, S. Arvindan, D. Parthiban, B. Saravanan, and M. Kalpana, "Natural aggregates used for light weight concrete —a Review," *IOP Conference Series: Materials Science and Engineering*, vol. 993, no. 1, Article ID 012042, 2020.

[3] D. L. C. Hao, R. A. Razak, M. Kheimi et al., "Artificial lightweight aggregates made from pozzolanic material: a review on the method, physical and mechanical properties, thermal and microstructure," *Materials*, vol. 15, no. 11, Article ID 3929, 2022.

[4] A. Tawfik, H. Awaad, T. M. El-Sokkary, and F. Abd El-Raoof, "Effect of SiC additions on bloating in clay from Toshka, Egypt," *Interceram—International Ceramic Review*, vol. 63, no. 4-5, pp. 198–201, 2014.

[5] E. A. Roces-Alonso, J. González-Galindo, and J. Estaire, "Experimental study on grain failure of lightweight expanded clay aggregate under uniaxial and biaxial load conditions," *Powder Technology*, vol. 383, pp. 542–553, 2021.

[6] Y. Wie and K. Lee, "Optimum bloating-activation zone of artificial lightweight aggregate by dynamic parameters," *Materials*, vol. 12, no. 2, Article ID 267, 2019.

[7] A. Ozguven and L. Gunduz, "Examination of effective parameters for the production of expanded clay aggregate," *Cement and Concrete Composites*, vol. 34, no. 6, pp. 781–787, 2012.

[8] A. V. Rodrigues and S. R. Bragança, "An evaluation of the increased expansion of clay aggregates fired at 1300°C to maximize lightness for non-structural concrete," *Boletín de la Sociedad Española de Cerámica y Vidrio*, vol. 62, no. 1, pp. 56–65, 2023.

[9] Y. L. Sravya, T. Manoj, and M. V. S. Rao, "Effect of temperature curing on lightweight expanded clay aggregate concrete," *Materials Today: Proceedings*, vol. 38, Part 5, pp. 3386–3391, 2021.

[10] Y. Jiang, T.-C. Ling, and M. Shi, "Strength enhancement of artificial aggregate prepared with waste concrete powder and its impact on concrete properties," *Journal of Cleaner Production*, vol. 257, Article ID 120515, 2020.

[11] S. Sivakumar and B. Kameshwari, "Influence of fly ash and LYTAG light weight aggregate on concrete," *International Journal of Applied Engineering Research*, vol. 10, no. 15, pp. 35843–35848, 2015.

[12] C. Burbano-Garcia, A. Hurtado, Y. F. Silva, S. Delvasto, and G. Araya-Letelier, "Utilization of waste engine oil for expanded clay aggregate production and assessment of its influence on lightweight concrete properties," *Construction and Building Materials*, vol. 273, Article ID 121677, 2021.

[13] C. Vilarinho, F. Castro, B. Mendonça, and C. Coelho, "Incorporation of wastes in lightweight aggregate of expanded clay for construction applications," ISWA World Congr. 2009, no. October, 2009.

[14] K. G. Lee, "Bloating mechanism of lightweight aggregate with the size," *Journal of the Korean Ceramic Society*, vol. 53, no. 2, pp. 241–245, 2016.

[15] S. A. Khan, S. M. U. Ghazi, H. Amjad, M. Imran, and R. A. Khushnood, "Emerging horizons in 3D printed cement-based materials with nanomaterial integration: a review," *Construction and Building Materials*, vol. 411, Article ID 134815, 2024.

[16] F. Hussain, S. A. Khan, R. A. Khushnood, A. Hamza, and F. Rehman, "Machine learning-based predictive modeling of sustainable lightweight aggregate concrete," *Sustainability*, vol. 15, no. 1, Article ID 641, 2023.

[17] K. H. Lee, K. G. Lee, Y. S. Lee, and Y. M. Wie, "Manufacturing and application of artificial lightweight aggregate from water treatment sludge," *Journal of Cleaner Production*, vol. 307, Article ID 127260, 2021.

[18] X. Shang, J. Chang, J. Yang, X. Ke, and Z. Duan, "Life cycle sustainable assessment of natural vs artificial lightweight aggregates," *Journal of Cleaner Production*, vol. 367, Article ID 133064, 2022.

[19] P. Ghisellini, X. Ji, G. Liu, and S. Ulgiati, "Evaluating the transition towards cleaner production in the construction and demolition sector of China: a review," *Journal of Cleaner Production*, vol. 195, pp. 418–434, 2018.

[20] P. Ren, T.-C. Ling, and K. H. Mo, "Recent advances in artificial aggregate production," *Journal of Cleaner Production*, vol. 291, Article ID 125215, 2021.

[21] A. J. Nath, R. Lal, and A. K. Das, "Fired bricks: CO_2 emission and food insecurity," *Global Challenges*, vol. 2, no. 4, Article ID 1700115, 2018.

[22] N. Liu and B. Chen, "Experimental study of the influence of EPS particle size on the mechanical properties of EPS lightweight concrete, Constr," *Construction and Building Materials*, vol. 68, pp. 227–232, 2014.

[23] A. R. Rafiza, A. Fazlizan, A. Thongtha, N. Asim, and M. S. Noorashikin, "The physical and mechanical properties of autoclaved aerated concrete (AAC) with recycled AAC as a partial replacement for sand," *Buildings*, vol. 12, no. 1, Article ID 60, 2022.

[24] M. Ikram, M. Ferasso, R. Sroufe, and Q. Zhang, "Assessing green technology indicators for cleaner production and sustainable investments in a developing country context," *Journal of Cleaner Production*, vol. 322, Article ID 129090, 2021.

[25] N. L. Lam, K. R. Smith, A. Gauthier, and M. N. Bates, "Kerosene: a review of household uses and their hazards in low- and middle-income countries," *Journal of Toxicology and Environmental Health, Part B*, vol. 15, no. 6, pp. 396–432, 2012.

[26] L. Wood, "Worldwide fly ash industry to 2026," 2026., https://www.globenewswire.com/news-release/2021/09/13/2295532/28124/en/Worldwide-Fly-Ash-Industry-to-2026-Increasing-Demand-from-the-Construction-Industry-is-Driving-Growth.html.

[27] P. Shafigh, M. A. Nomeli, U. J. Alengaram, H. B. Mahmud, and M. Z. Jumaat, "Engineering properties of lightweight aggregate concrete containing limestone powder and high volume fly ash," *Journal of Cleaner Production*, vol. 135, pp. 148–157, 2016.

[28] I. B. Muhit, S. S. Ahmed, M. F. Zaman, and M. S. Ullah, "Effects of multiple supplementary cementitious materials on workability and strength of lightweight aggregate concrete," 2017, [Online]. Available: https://api.semanticscholar.org/CorpusID:226252513.

[29] M. H. Khalid, B. Alshameri, and U. Abid, "Application of Kriging for development of SPT N value contour maps and USCS-based soil type qualitative contour maps for Islamabad, Pakistan," *Environmental Earth Sciences*, vol. 80, no. 11, pp. 1–13, 2021.

[30] C09 Committee, "Specification for coal fly ash and raw or calcined natural pozzolan for use in concrete," pp. 1–5

[31] T. Officials, "Specification for Portland cement," *ASTM International*, vol. 70, no. Reapproved, pp. 1-2, 2004.

[32] C. M. Riley, "Relation of chemical properties to the bloating of clays," *Journal of the American Ceramic Society*, vol. 34, no. 4, pp. 121–128, 1951.

[33] ASTM D4318-10, "Standard test methods for liquid limit, plastic limit, and plasticity index of soils," *American Society for Testing and Materials*, pp. 1–16, 2010.

[34] ASTM D-427, "Standard test method for shrinkage factors of soils by the mercury method," *ASTM International*, vol. i, pp. 1–4, 2004.

[35] J. M. Moreno-Maroto and J. Alonso-Azcárate, "Plastic limit and other consistency parameters by a bending method and interpretation of plasticity classification in soils," *Geotechnical Testing Journal*, vol. 40, no. 3, Article ID 20160059, 2017.

[36] F. Hussain, F. Rehman, R. A. Khushnood, S. A. Khan, and A. Hamza, "Study of physical and mechanical behavior of artificial lightweight aggregate made of Pakistani clays," *Construction and Building Materials*, vol. 378, Article ID 131103, 2023.

[37] T. Y. Lo, H. Cui, S. A. Memon, and T. Noguchi, "Manufacturing of sintered lightweight aggregate using high-carbon fly ash and its effect on the mechanical properties and microstructure of concrete," *Journal of Cleaner Production*, vol. 112, pp. 753–762, 2016.

[38] Q. Du, Q. Sun, J. Lv, and J. Yang, "Use of preplaced casting method in lightweight aggregate concrete," *Advances in Materials Science and Engineering*, vol. 2017, Article ID 7234761, 7 pages, 2017.

[39] S. Siddique, H. Kim, H. Son, and J. G. Jang, "Characteristics of preplaced aggregate concrete fabricated with alkali-activated slag/fly ash cements," *Materials*, vol. 14, no. 3, Article ID 591, 2021.

[40] ASTM: C937, "Standard Specification for Grout Fluidifier for Preplaced-Aggregate Concrete," *ASMT International*, vol. i, no. c, pp. 10–12, 2016.

[41] J. M. Moreno-Maroto and J. Alonso-Azcárate, "What is clay? A new definition of 'clay' based on plasticity and its impact on the most widespread soil classification systems," *Applied Clay Science*, vol. 161, pp. 57–63, 2018.

[42] C. Molinari, C. Zanelli, G. Guarini, and M. Dondi, "Bloating mechanism in lightweight aggregates: effect of processing variables and properties of the vitreous phase," *Construction and Building Materials*, vol. 261, Article ID 119980, 2020.

[43] M. C. S. Nepomuceno and P. D. Silva, "Experimental evaluation of cement mortars with phase change material incorporated via lightweight expanded clay aggregate," *Construction and Building Materials*, vol. 63, pp. 89–96, 2014.

[44] A. Shokri, "Using Mn based on lightweight expanded clay aggregate (LECA) as an original catalyst for the removal of NO_2 pollutant in aqueous environment," *Surfaces and Interfaces*, vol. 21, Article ID 100705, 2020.

[45] Astm:C29/C29M-09, "Standard test method for bulk density ('Unit Weight') and voids in aggregate," *ASTM International*, vol. i, no. c, pp. 1–5, 2009.

[46] EN 13055-1, "Lightweight aggregates for concrete, mortar and grout," 2016.

[47] F. A. Torralvo, C. F. Pereira, and O. F. Piqueras, "By-products from the integrated gas combined cycle in IGCC systems," in *Integrated Gasification Combined Cycle (IGCC) Technologies*, pp. 465–494, Elsevier, 2017.

[48] R. de Gennaro, P. Cappelletti, G. Cerri et al., "Campanian Ignimbrite as raw material for lightweight aggregates," *Applied Clay Science*, vol. 37, no. 1-2, pp. 115–126, 2007.

[49] Astm C127, A. S. T. M., "Standard test method for relative density (specific gravity) and absorption of coarse aggregate," ASTM West Conshohocken, PA, pp. 1–5, 2015.

[50] ASTM C39/C39M, "Standard test method for compressive strength of cylindrical concrete specimens 1 this standard is for educational use only," Annu. B. ASTM Stand., no. C, pp. 1-7, doi: 10.1520/C0039, 2010.

[51] S. Specification and iTeh Standards, "iTeh Stand." vol. i, pp. 1-2, 2023, doi: 10.1520/C0055-22.2, 2023.

[52] L. K. A. Sear, J. Dews, B. Kite, F. C. Harris, and J. F. Troy, "Abrams law, air and high water-to-cement ratios," *Construction and Building Materials*, vol. 10, no. 3, pp. 221–226, 1996.

[53] P. L. N. Fernando, M. T. R. Jayasinghe, and C. Jayasinghe, "Structural feasibility of expanded polystyrene (EPS) based lightweight concrete sandwich wall panels," *Construction and Building Materials*, vol. 139, pp. 45–51, 2017.

[54] Astm: C138/C138M-13, "Standard test method for density (unit weight), yield, and air content (gravimetric)," *ASTM International*, vol. i, pp. 23–26, 2013.

[55] D. Rumsys, E. Spudulis, D. Bacinskas, and G. Kaklauskas, "Compressive strength and durability properties of structural lightweight concrete with fine expanded glass and/or clay aggregates," *Materials*, vol. 11, no. 12, Article ID 2434, 2018.
[56] ECS, "Eurocode 2- design of concrete structures- Part 1–1: general rules and rules for buildings," *Data Structures Tutorial*, vol. 3, Article ID 230, 2006.
[57] ASTM 900-06, "Standard test method for pullout strenght of hardened concrete," *American Society for Testing and Materials*, vol. 1, pp. 1–10, 1999.
[58] J. A. Bogas, R. Nogueira, and N. G. Almeida, "Influence of mineral additions and different compositional parameters on the shrinkage of structural expanded clay lightweight concrete," *Materials & Design (1980-2015)*, vol. 56, pp. 1039–1048, 2014.
[59] ASTM C 597-02, "Pulse velocity through concrete," *United States American Society for Testing and Materials*, vol. 04, no. 2, pp. 3–6, 2016.
[60] X. Liu, D. Sun, J. Liao et al., "Quality evaluation of lightweight cellular concrete by an ultrasound-based method, Front," *Frontiers of Structural and Civil Engineering*, vol. 16, no. 9, pp. 1170–1182, 2022.
[61] J. A. Bogas, M. G. Gomes, and A. Gomes, "Compressive strength evaluation of structural lightweight concrete by non-destructive ultrasonic pulse velocity method," *Ultrasonics*, vol. 53, no. 5, pp. 962–972, 2013.
[62] ASTM C469-11, "Standard test method for splitting tensile strength of cylindrical concrete specimens," *ASMT International*, vol. i, pp. 545–545-3, 2008.
[63] C. C. Test, T. Drilled, and C. Concrete, "Standard test method for flexural strength of concrete (using simple beam with third-point loading) 1," *Hand*, vol. 2, no. C, pp. 1–4, 2010.
[64] J. A. Bogas and A. Gomes, "Compressive behavior and failure modes of structural lightweight aggregate concrete–characterization and strength prediction," *Materials & Design (1980-2015)*, vol. 46, pp. 832–841, 2013.
[65] M. Słowik, "The analysis of failure in concrete and reinforced concrete beams with different reinforcement ratio," *Archive of Applied Mechanics*, vol. 89, no. 5, pp. 885–895, 2019.
[66] P. Shafigh, L. J. Chai, H. B. Mahmud, and M. A. Nomeli, "A comparison study of the fresh and hardened properties of normal weight and lightweight aggregate concretes," *Journal of Building Engineering*, vol. 15, pp. 252–260, 2018.